Optics & Laser Technology 152 (2022) 108105

Contents lists available at ScienceDirect

Optics and Laser Technology

journal homepage: www.elsevier.com/locate/optlastec

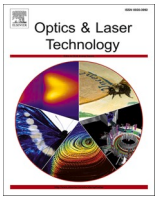

Optical switching in glass fibre composite

Christopher Holmes [a,*], Mike Godfrey [b], Paolo L. Mennea [a], Daniel J. Bull [b], Janice Dulieu-Barton [c]

[a] Optoelectronics Research Centre, University of Southampton, UK
[b] School of Engineering, University of Southampton, UK
[c] Bristol Composites Institute, University of Bristol, UK

ARTICLE INFO

Keywords:
Advanced composite
Optical switch
Planar optics

ABSTRACT

We demonstrate for the first time the reconfigurability of optical signals within advanced laminated composite. The approach employs an ultra-thin planar optical circuit, embedded within glass fibre reinforced polymer (GFRP) that switches an optical input though Ohmic heating. This advance highlights new opportunities for optical reconfigurability within advanced composites, enabling data transmission redundancy and a consideration of branching optical fibre architectures.

1. Introduction

Embedding optical fibres into laminated composites, such as glass fibre and carbon fibre reinforced polymer is a mature technology, having had considerable developments over the past several decades [1–3]. In these arrangements, optical fibres are typically located between the plies of the composite laminate and due to their small cross-section offer minimal intrusion, maintaining a high degree of mechanical integrity. Optical fibre offers many other advantages including an ability to multiplex many sensor elements along its length, immunity to electromagnetic interference and operation in extreme environments, such as elevated temperatures and pressures used during composite cure.

A significant challenge with embedding optical fibre within composite laminates is its susceptibility to single point failure; meaning, if the optical fibre is damaged within the composite, there is currently no feasible route for repair. Each sensing element along an embedded optical fibre is serial sequenced point-to-point. A common, single route of communication exists from the sensor to the external optical interrogation system, so that damage in a single location along the optical fibre between these two points results in a paralysis of all sensors downstream from the damage location.

Optical telecommunication networks once experienced similar limitations. In their infancy, *trans*-oceanic links operated in a simple point-to-point configuration. However, modern day subsea network architectures are more complex and have branching nodes to connect either full fibre pairs or portions to a trunk and/or branch fibre [4]. This permits reconfigurability, which has transformed the reliability of our subsea communication network, offering redundancy to bypass cable damage. More broadly, optical telecommunication infrastructure adopts mesh network topologies that contains optical transport equipment capable of switching incoming to outgoing optical fibres. Our concept is to translate a similar architecture, creating reconfigurable optical fibre sensor networks within high-value laminated composites, such as those used to build modern aircraft and wind turbine blades. Conceptually, many optical switches could be distributed within a composite structure, each reconfigured to address many different optical fibres, each contain many different sensor elements.

In optical telecommunications, mesh networks are realised through optoelectronic switches, which can freely reroute signals. Conceptually, optical switches could redirect signals around damaged sections of composite structures, maintaining greater network integrity. However, the translation of such an architecture into a composite structure is not trivial. Commercial switches are typically mechanical, they are large and bulky and simply too big to embed between the ply layers of a composite material. Their presence would compromise the mechanical strength of the composite. Integrated photonics offer high efficiency small footprint optical switching [5]. However, typical substrate thicknesses used, for example in silicon, are of the order 675 μm and require yet thicker packaging profiles when coupled to silica optical fibre [6].

Despite being less power efficient for switching, silica-based planar photonics can be thinned to < 40 μm and has simpler butt-coupling solutions, resulting in negligible mechanical degradation to composite

* Corresponding author.
E-mail address: christopher.holmes@soton.ac.uk (C. Holmes).

https://doi.org/10.1016/j.optlastec.2022.108105
Received 17 September 2021; Received in revised form 22 February 2022; Accepted 21 March 2022
Available online 28 March 2022

material [7]. From the perspective of structural integrity of large composite structures, this is of primary importance. Hence, the functionality of composite materials is enhanced by providing an ability for optical rerouting using switches. (It should be noted that the intention is not to improve the performance of the optical switch by embedding it into a laminated composite.) Here we build upon recently shown feasibility of embedded ultra-thin silica planar optics [7,8], developing an ultra-thin optical switch that can service optical fibre in a 2x2 configuration. This is the first report of an ultra-thin optoelectronic switch embedded within a laminated composite and offers the potential for optical rerouting in large composite structures. The switch utilises a planar optical circuit containing a Mach-Zehnder Interferometer (MZI) tuned electrically through a localised Ohmic heating, conceptually illustrated in Fig. 1 **(a)**. This work increases optical complexity and capability in composite material. It is envisaged that further evolution of design complexity will offer yet further multifunctionality to the composite for sensing [7], communication [9,10] and local computation [11–13].

2. Fabrication methodology

The MZI was fabricated using cleanroom and laser-based manufacture techniques. It is composed of a silicon wafer with 15 μm thermally grown oxide. The thick oxide layer (SiO_2) acts as an optical underclad. A core and overclad layer are subsequently deposited, through flame hydrolysis deposition (FHD). The core layer was designed to be UV photosensitive through doping the silicate with germanium and boron, this allowed waveguides to be written into the core layer through direct UV laser writing. This process used a frequency doubled continuous wave Ar-ion laser at 244 nm wavelength, the beam was focused to a 7 μm spot and traversed in the core layer [14]. The silicon wafer was diced to a 10 mm by 20 mm chip and hydrogenated for 1 week to further enhance photosensitivity. The MZI consisted of a pair of waveguides offset by 127 μm and two X-couplers of crossing angle 2.2°. To create a pathlength imbalance a 175 nm thick nichrome (NiCr 80/20) heating filament was deposited over one arm of the MZI through photolithography and e-beam evaporation, shown in Fig. 1.

To reduce the effect of embedding the planar optical circuit on the mechanical performance of the composite, it was necessary to reduce its thickness by physically machining [7]. Here the majority of the silicon was removed with a rastering sequence through the use of a Loadpoint MicroAce dicing saw and a synthetic diamond impregnated resin blade (DISCO R07-SD400 series). The kerf of the blade was 250 μm, a raster pitch of 90 μm, a feed rate of 5 mms^{-1} and a spindle speed of 25,000 RPM were used. The resulting surface quality had < 3 μm waviness. Alternative physical machining techniques such as lapping and polishing could be considered. Significant compressive residual stresses between the thermal oxide and the FHD layers resulted in warping of the chip with partial removal of the silicon [15], and cracking of the silica layer with complete removal of the silicon. For this reason, not all the silicon was removed: the chip was embedded into the composite with a final total thickness of 300 μm, illustrated in Fig. 2.

The composite was fabricated from RP-528 unidirectional GFRP epoxy prepreg from PRF composites. GFRP was chosen due to its low electrical conductivity to minimise the risk of current leakage and short circuits; however, implementation of an insulating coating on the electrical contacts by simply encapsulating could facilitate the use within a carbon fibre based composite. The laminate ($142 \times 142 \times 1$ mm) consisted of 4 plies with a $[0/90]_s$ layup; the zero direction was parallel to the optical waveguides, illustrated in Fig. 1 (a). The chip and embedded wires were placed between the central plies. The wires were lacquered

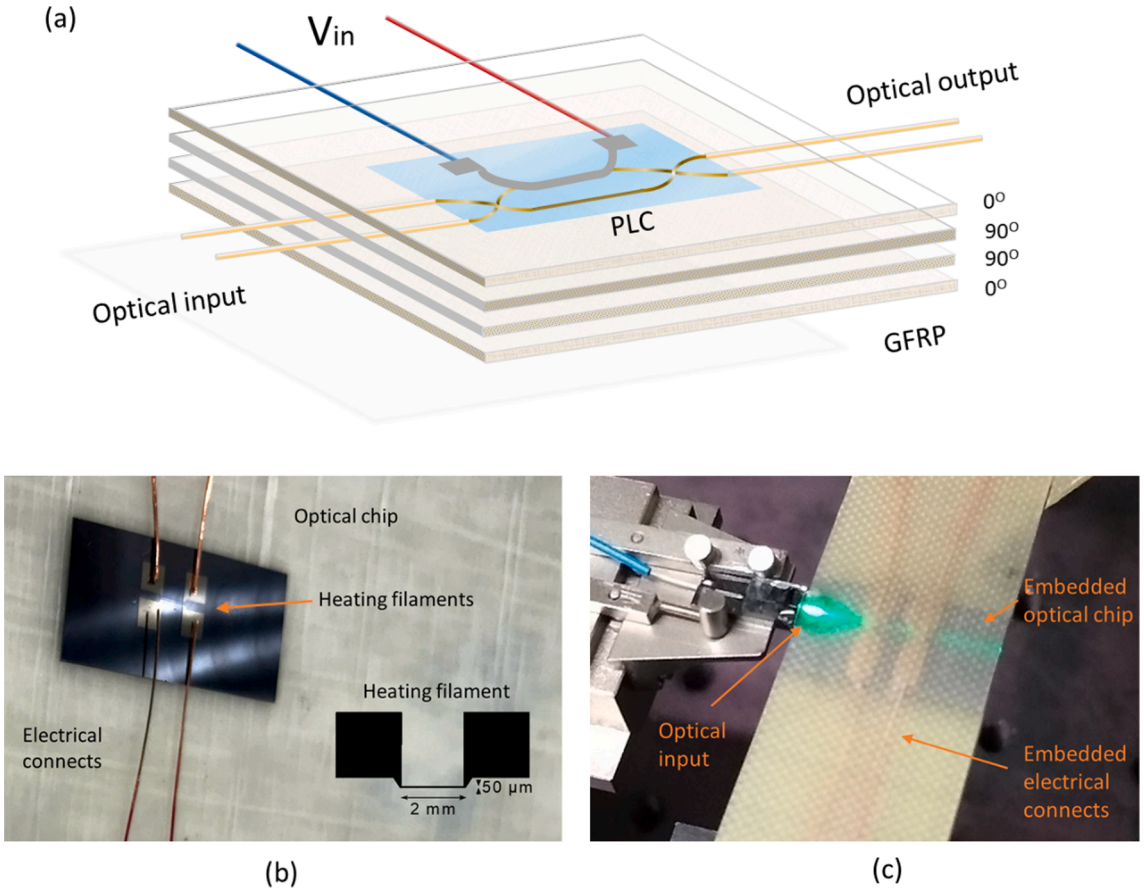

Fig. 1. (a) Conceptual image of integrated optical chip (Photonics Lightwave Circuit, PLC) embedded in glass fibre reinforced polymer, the chip contains a Mach-Zehnder switch with resistive heater centred over one arm. Photograph of optical switch (b) during composite layup and (c) embedded within glass fibre polymer.

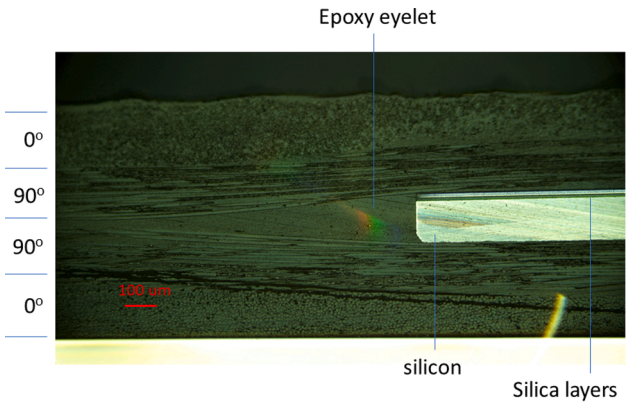

Fig. 2. Cross-section of planar optical switch embedded within 4-layer GFRP, with a $[0/90]_s$ layup.

single-core copper, attached to the electrical contacts using two-part conductive silver epoxy (Chemtronics, CW2400). The composite was vacuum-bagged and debulked at room temperature for 10 min before curing in an autoclave under vacuum at 120 °C for 1 h at 5 bar gauge pressure. After the cure was complete the laminate was diced, with the cuts intersecting the two shorter edges of the chip to enable optical coupling. The resulting device, illustrated in Fig. 1 **(b)**, contained two MZI switches separated by 1.127 mm, with two separate heating filaments. Electrical continuity was observed between the two filaments suggesting electrical bridging occurred during fabrication. Here adjacent terminals on the adjacent filaments showed a resistance of 11 Ω and 1.2 Ω respectively. The electrical resistances of the heating elements were 711 Ω and 706 Ω respectively. When wired in parallel, the resistance was 704 Ω. Two heaters were simultaneously actuated through wiring them in parallel.

3. Demonstration of optical switching

To investigate optical power splitting of the MZI one of the input waveguides was illuminated with 1306 nm laser light (Agilent, 81654A), and the output (Arm #1 and Arm #2) imaged with a near-infrared camera (Raptor Photonics, OW1.7-VS-CL-640). Power slitting was observed subject to different voltages, driven with a dual power direct current supply (Thurlby, Model 30 V-1A), illustrated in Fig. 3.

Optical power splitting, shown in Fig. 3 **(c)**, was calculated by integrating the output from the captured images. It shows 2π tuning of the MZI over 1.65 W (34 V). The thermal coefficient of resistivity for nichrome is $4.1 \times 10^{-4}\ K^{-1}$, meaning for an optical path length of 2 mm, a 2π phase change would correspond to a temperature change of ~ 100 K, assuming a thermo-optic coefficient of $6.5 \times 10^{-6}\ K^{-1}$. This relates to a 1% underestimation in power resulting from resistance variation.

From Fig. 3 (b) and (c) it is noted that full power extinction for Arm #2 is not obtained, there remains ~ 10% power output. This can be explained in part due to non-symmetric splitting ratios of the X-couplers that form the MZI. Ensuring symmetric optical power splitting shall be the target for future development. Fig. 3(c) depicts the optical outputs of Arm#1 and Arm#2 for a series of electrical powers. For continuous Ohmic heating the optical outputs could be maintained for all input powers. To quantify temporal response the maximum power for switching was investigated, illustrated in Fig. 4.

Fig. 4 shows captured thermal images (FLIR, ETS320) prior (a), during (b) and immediately after (c) 1-second of Ohmic heating (potential difference set to 23 V). It shows localised heating and heat dissipation for the switch.

To observe the temporal response of the switch, a 10 Hz square wave was created on a signal generator (Tektronix, AFG3021B) and amplified (New Focus, 3211) from 0 V to 23 V (0.75 W). This range was chosen as the power-on segment provides an approximate π-phase change for the MZI. The optical output from Arm #1 was measured using an InGaAs amplified detector (Thorlabs, PDA 10CS-EC) with 17 MHz bandwidth, using an Olympus x20 objective. The output from the detector was triggered on a digital oscilloscope (Tektronix, TBS 1072B-EDU), shown in Fig. 4 **(d)-(f)**. This shows an e^{-1} turn-off response of 477 ± 2 μs and a turn-on response of 1.13 ± 0.01 ms. It is observed that heat dissipation has an influence on the operation of the switch. This is shown in Fig. 4 (d) and (e), where the temporal response has two parts, a fast initial response corresponding to a localised thermal gradient and a smaller drift corresponding to bulk heating until thermal equilibrium is reached.

The temporal response of the buried heating filament is faster than previous observations, by a factor of two [16]. Previous observations for similar, non-buried optical circuits had a response of 1.02 ms for lower heat dissipation of 500 mW. The faster turn-off response may be attributed to greater thermal conductivity, most notably on the top side of the chip.

Clearly the heating effects result in temperatures much lower than those that would affect the structural performance of the GFRP. However, this is an external measurement and hence a means of assessing the local temperature change inside the composite is required. To consider further the optical response in relation to planar chip design and the localised heating caused by the switching, a 3D finite element heat transfer model was developed, which provides insight into the effect of the silicon layer on switching performance and localised temperature elevation (see Fig. 5). The latter is important as localised temperature evolutions may cause softening of the epoxy resin in the GFRP material and reductions in structural performance. Here, the silica layer was modelled as a flat plate 10 mm × 20 mm × 40 μm assigned with Corning 7940 fused silica from the COMSOL database. The silicon layer was modelled as a flat plate adjacent to the underneath of the silica with the dimensions 10 mm × 20 mm × 260 μm and the assigned thermal properties from the COMSOL database. The chip was surrounded by GFRP, assumed to have isotropic thermal properties, as the conductivity of the glass fibre and the epoxy resin are both low. Hence thermal conductivity was set to $k = 0.35\ Wm^{-1}K^{-1}$, with the scaler quantities of density set to $\rho = 1870\ kgm^{-3}$ and specific heat capacity set to $C_p = 1170\ Jkg^{-1}K^{-1}$ [17–19]. The GFRP layer was dimensioned as 142 mm × 142 mm × 1 mm in the case with no silicon and 1.26 mm thick in the case with the silicon to maintain the same thickness of GFRP surrounding the chip in both cases. The chip was positioned centrally in the GFRP and the assembly was formed as a union object. The external surface of the GFRP was subject to a convective heat flux with a heat transfer coefficient of $5\ Wm^{-2}K^{-1}$ and an external temperature of 20 °C. A line heat source was applied in the centre of the top face of the silica layer, representing the NiCr heating element in the demonstrated switch. The line segment was defined to be 2 mm long and provided a nominal heating power of $100\ Wm^{-1}$. Here, switching performance is assessed using the temperature difference between adjacent waveguides of the MZI (i.e. Arm #1 and Arm #2) for given heating in its steady state.

To assess switching, the average temperature along the two waveguides (i.e. Arm #1 and Arm #2) is required. To achieve this 2 mm long cut-lines, both situated 20 μm below the surface of the silica (i.e. in line with the waveguide core). The first cut-line was positioned directly beneath the line heat source, and the second was translated horizontally by 127 μm, thus representing each of the two arms.

A tetrahedral mesh was applied to the entire model. The minimum element size for the GFRP, silica and silicon was defined as 10 μm globally, with the upper limit set automatically by COMSOL. Local refinement was applied to the region surrounding the line heat source with a minimum element size defined as 1 μm. This mesh was confirmed to converge by recording the average temperature in the silica layer for a variety of different element sizes.

The local composite temperature, in steady state, for the switch with silicon is lower than that with silica only, illustrated in Fig. 5. This appears to be a result of the thermally conductive silicon laterally

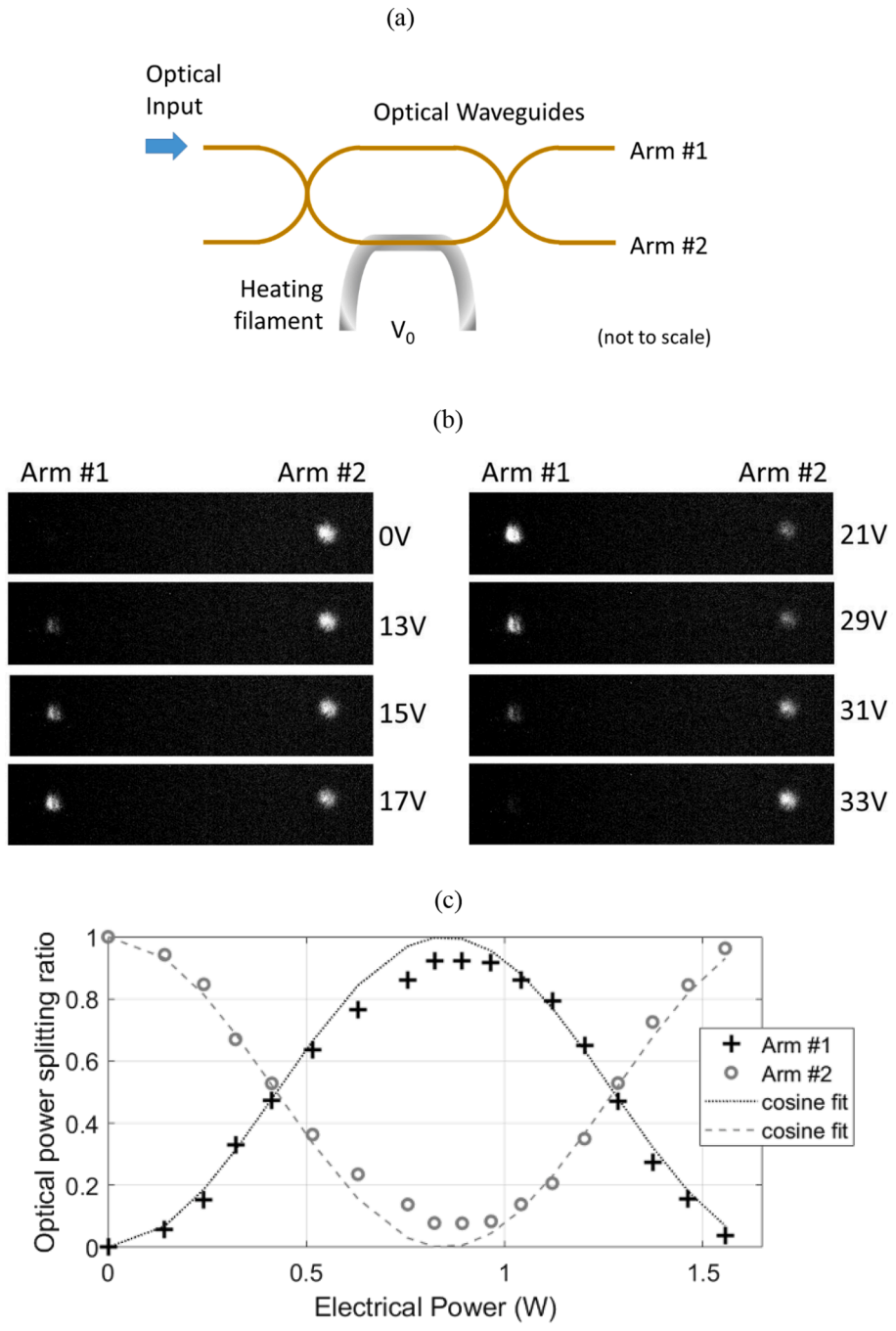

Fig. 3. (a) schematic of the experimental set-up and (b) optical output of Arm #1 and Arm #2 as imaged upon near-infrared camera subject to applied voltage (c) Switching of optical power between Arm #1 and Arm #2 subject to electrical heating.

dissipating the heat. For the waveguide directly beneath the heating element, the maximum temperature reduced from 308.8 °C to 69.1 °C with the introduction of the silicon layer. More importantly, however, the temperature difference between the two arms also reduced with the inclusion of the silicon layer. The mean temperature in the heated and unheated arms in the case without the silicon layer was 291.6 °C and 249.6 °C respectively, and in the case with the silicon layer, the respective mean temperatures were 68.0 °C and 52.2 °C, illustrated in Fig. 6. Therefore, the mean temperature difference between the two arms dropped from 42.0 °C to 15.8 °C with the inclusion of the silicon layer when a power of 100 W/m was applied.

The efficiency difference between the two scenarios (i.e., power required to achieve the same average temperature difference) was determined. In the case of the silica only chip, to achieve the same average temperature differential as with the silicon, a lower heating power of 35 W/m was required, suggesting a 3-times improvement over the silicon configuration. However, as shown in Fig. 5(c), the temperature of the composite is unacceptably high for this silica-only configuration, suggesting that silicon or other thermally conductive layer is important for thermal management of the switch.

4. Discussion

The first demonstration of an optoelectronic switch embedded in a laminated composite is presented. This highlights the potential for new optoelectronic functionality for composite structures, including large-

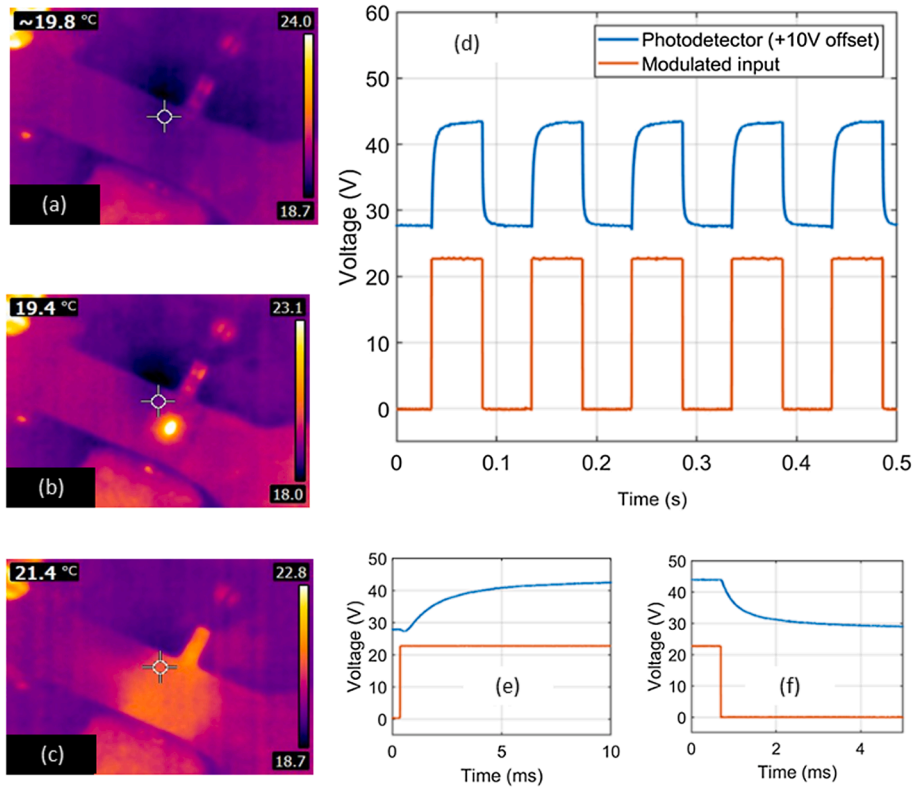

Fig. 4. Infrared camera images showing the (a) before (b) during and (c) ~ 1 s after Ohmic heating. Temporal response of the embedded optical switch, showing (d) 10 Hz modulation (e) warm-up feature of heating filament and (f) cool-down.

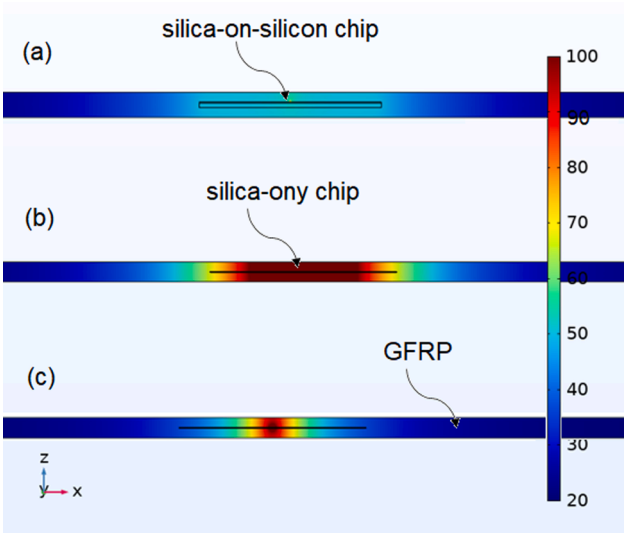

Fig. 5. The steady state temperature distribution in cross-section, with (a) 100 W/m heating applied to measured silica-on-silicon chip (b) 100 W/m heating for silica only chip and (c) 35 W/m heating for silica only chip (this power has equivalent temperature difference between waveguides as measured for silica-on-silicon chip supplied by 100 W/m).

scale embedded sensor networks, for structural health monitoring. Hence it is demonstrated that the switch adds new optical functionality into laminated composite material and importantly the process of thinning the chip and embedding it into a composite material does not impede its operation. Optical switching is complementary to ongoing advances in electronic multifunctionality [20] in composites, that consist of lithographically patterned polyimide with copper. Electrical actuation could also be developed in future applications for add-drop functionality, enabling spectral multiplexed signals to be routed within composites using filtering approaches, which include those based upon Ohmic heating [16].

The insertion loss for the switch can be divided into three parts (i) propagation loss, (ii) geometric loss and (iii) fibre-to-chip coupling loss. Propagation losses in the platform have been measured to be 0.2 dB/cm [21], summing to an approximate contribution of 0.4 dB for a single switch. Geometric losses due to the step-index X-coupler are understood to be of the order of 1 dB [22]. Fibre-to-chip loss is the greatest contributor, due largely to alignment errors and can be up to 4 dB [23]. Improvements could potentially be achieved through fiberizing such a design, perhaps through use of a flat fibre platform which would permit a similar planar construction and heating assembly reported [24]. A MZI formed using commercial fibre couplers would have an excess loss of $<$ 0.3 dB, which is considered a feasible target for future development.

The efficiency of the demonstrated switch could be further developed. Currently, for the switch to operate in one of its two states, requires an 803 mW supply of power. This is greater than commercial optical switches used in data centres. The FEA simulations indicate that a complete removal of the silicon substrate would result in a 3-fold increase in efficiency. However, Fig. 5 shows that whilst silica-only designs are more efficient at switching they increase the local temperature of the composite dramatically, which would affect composite performance. This means that the silicon substrate (or inclusion of another material of appropriate thermal conductivity) is an essential feature for an embedded thermo-optic switch in planar doped silica. The silicon acts as a heatsink, dissipating the power and thus managing the temperature in the composite. Further design improvements to manage composite temperature could include: increasing the arm lengths of the MZI, which would linerarly scale down the average temperature difference required (assuming linear thermal expansion); increase the separation of the MZI arms; positioning of the heating element (e.g. within the core layer); increasing the width of the optical chip; use of other thermally

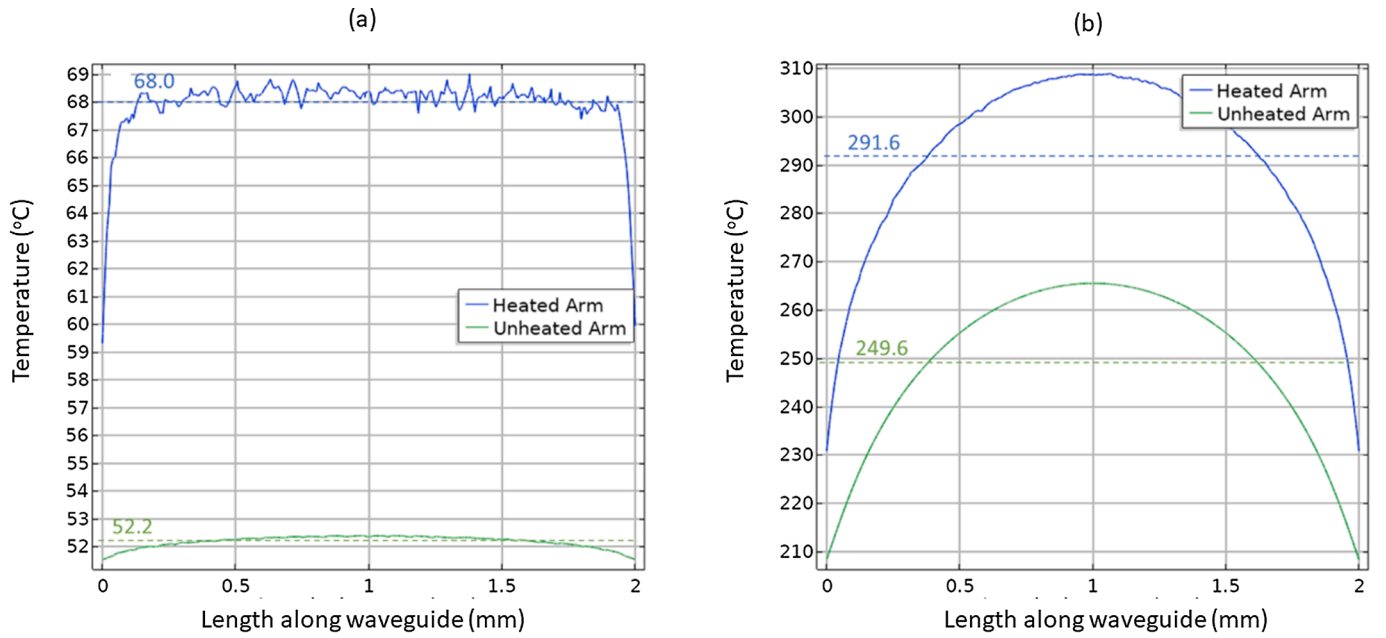

Fig. 6. The temperature along arm #1 (heated arm) and arm #2 (unheated arm), for Ohmic heating of 100 W/m considering a geometry where (a) with the silicon substrate remains and (b) without the silicon substrate (The variations in response are an artefact of the mesh density). Dashed lines indicate average temperature observed by each arm of the MZI.

conducting and thermally insulating layers.

To further improve efficiency and thermal management, future designs could incorporate thermal or optically switchable materials [25]. An all-optical switch would allow control through a separately injected light signal [26]. Such a designs would remove the need for electrical powering.

It should be noted that the switch design, based upon an integrated MZI, is inherently insensitive to ambient temperature and pressure changes. This means the switch can be integrated and operate as expected under the real-world conditions a composite structure is expected to experience. The reason for the insensitivity arises due to the two waveguide arms being in physical proximity (they are only 127 μm apart) and symmetrical in length. A phase change between these arms is needed in order to initiate switching. Due to the proximity of the arms to each other temperature and pressure changes would approximately be equivalent. Bending and loading would have a similar response. Twisting, could result in a pathlength imbalance, however, the scenario that will result in the largest path length imbalance would be where the axis of twisting is aligned with one of the arms, thereby the aligned arm would experience no length change and the other arm would be subjected to a positive strain. The angle required to achieve π phase change in this scenario can be geometrically calculated to be ≈20°, which is a much larger torsional deformation than would be expected in the majority of composite structures. Further to this, any small influence could be negated through appropriate design in network topology (i.e. location of the switches) or feedback control of actuation.

5. Conclusion

The first planar optical switch embedded into an advanced composite is presented. The optoelectronic switch highlights new optical functionality in advanced composites, as well as potential routes to overcome current limitations of single-point failure through the building blocks for fully reconfigurable optical mesh networks. This is the first demonstration of an optical switch embedded within a laminated composite material. It provides a completely new optical functionality that opens up new potential optical topologies in composite structures, including efficient usage of sensor interrogation and fibre cabling and an ability for optical rerouting or obviate any damaged optical fibre segments.

We demonstrate an integrated Mach-Zehnder switch embedded withing glass fibre reinforced polymer, driven electrically through Ohmic heating to create an optical pathlength imbalance. We obtain optical switching at 1306 nm wavelength (O-band), driven by 803 mW of electrical power with an e^{-1} switching response of 477 ± 2 μs. It is observed that thermal management to ensure the composite material does not reach undesirable temperatures can come at the cost of switching efficiency. However, the offering of this advance is not efficiency of an optical switch but the new functionality derived for laminated composite materials.

CRediT authorship contribution statement

Christopher Holmes: Conceptualization, Data curation, Formal analysis, Funding acquisition, Investigation, Methodology, Project administration, Resources, Software, Supervision, Validation, Visualization, Writing – original draft, Writing – review & editing. **Mike Godfrey:** Data curation, Formal analysis, Investigation, Methodology, Software, Validation, Visualization, Writing – original draft. **Paolo L. Mennea:** Investigation, Software, Validation, Visualization, Writing – original draft. **Daniel J. Bull:** Validation, Visualization, Writing – original draft. **Janice Dulieu-Barton:** Funding acquisition, Methodology, Project administration, Validation, Visualization, Writing – review & editing.

Declaration of Competing Interest

The authors declare that they have no known competing financial interests or personal relationships that could have appeared to influence the work reported in this paper.

Acknowledgements

The research has been partly developed under EPSRC “Roll-2-Roll (R2R) manufacture of multilayer planar optics’, EP/V053213/1. For the purpose of open access, the author has applied a creative commons

attribution (CC BY) licence (where permitted by UKRI, 'open government licence' or 'creative commons attribution no-derivatives (CC BY-ND) licence' may be stated instead) to any author accepted manuscript version arising. The authors thank James Gates for maintenance of the direct UV writing systems and Rex Bannerman for building the near-infrared characterization set-up.

References

[1] M. Majumder, T.K. Gangopadhyay, A.K. Chakraborty, K. Dasgupta, D. K. Bhattacharya, Fibre Bragg gratings in structural health monitoring-Present status and applications, Sensors Actuators, A Phys. 147 (1) (2008) 150–164, https://doi.org/10.1016/j.sna.2008.04.008.

[2] P. Taylor, C. Boller, Next generation structural health monitoring and its integration into aircraft design Next generation structural health monitoring and its integration, Int. J. Syst. Sci. 31 (August 2013 2010) 37–41, https://doi.org/10.1080/00207720050197730.

[3] G. Zhou, L.M. Sim, Damage detection and assessment in fibre-reinforced composite structures with embedded fibre optic sensors-review, Smart Mater. Struct. 11 (6) (2002) 925–939.

[4] N. S. Bergano, B. Dean, L. Garrett, M. E. Kordahi, H. Li, and B. Nyman, "Submerged plant equipment," in *Undersea Fiber Communication Systems: Second Edition*, Elsevier Ltd, 2016, pp. 421–464.

[5] R. Soref, "Tutorial: Integrated-photonic switching structures," *APL Photonics*, vol. 3, no. 021101, 2018, doi: 10.1063/1.5017968.

[6] G. Son, S. Han, J. Park, K. Kwon, K. Yu, High-efficiency broadband light coupling between optical fibers and photonic integrated circuits, Nanophotonics 7 (12) (2018) 1845–1864.

[7] C. Holmes, M. Godfrey, D. J. Bull, and J. Dulieu-Barton, "Real-time through-thickness and in-plane strain measurement in Carbon Fibre Reinforced Polymer composites using planar optical Bragg gratings," *Opt. Lasers Eng.*, vol. 133, no. 106111, 2020.

[8] S. Kefer, T. Sauer, S. Hessler, M. Kaloudis, B. Schmauss, R. Hellmann, Robust polymer planar bragg grating sensors embedded in commercial-grade composites, Polymers (Basel) 12 (3) (2020) 1–12, https://doi.org/10.3390/polym12030715.

[9] R.G. Hunsperger, *Integrated Optics : Theory and Technology*, Sixth Edit. Springer, Springer, New York, 2009.

[10] L.A. Coldren, S.W. Corzine, M.L. Mashanovitch, Diode Lasers and Photonic Integrated Circuits, Wiley & Sons, 2011.

[11] K.-I. Kitayama, M. Notomi, M. Naruse, K. Inoue, S. Kawakami, A. Uchida, Novel frontier of photonics for data processing—photonic accelerator, APL Photonics 4 (9) (2019) 090901, https://doi.org/10.1063/1.5108912.

[12] T.W. Hughes, M. Minkov, I.A.D. Williamson, Y. Shi, S. Fan, Training of photonic neural networks through in situ backpropagation, Optica 5 (7) (2018) 864–871, https://doi.org/10.1364/CLEO_AT.2019.JF3F.2.

[13] Y. Shen, N.C. Harris, S. Skirlo, M. Prabhu, T. Baehr-Jones, M. Hochberg, X. Sun, S. Zhao, H. Larochelle, D. Englund, M. Soljačić, Deep learning with coherent nanophotonic circuits, Nat. Photon 11 (7) (2017) 441–446, https://doi.org/10.1038/nphoton.2017.93.

[14] G.D. Emmerson, S.P. Watts, C.B.E. Gawith, V. Albanis, M. Ibsen, R.B. Williams, P.G. R. Smith, Fabrication of directly UV-written channel waveguides with simultaneously defined integral Bragg gratings, Electron. Lett. 38 (24) (2002) 1531, https://doi.org/10.1049/el:20021056.

[15] C. Holmes, J.C. Gates, P.G.R. Smith, Integrated optical differential pressure transducers achieved using thin buckled silica membranes and direct UV written planar Bragg gratings, Sensors Actuators A Phys. 168 (1) (2011) 14–21, https://doi.org/10.1016/j.sna.2011.03.030.

[16] C. Holmes, D.O. Kundys, J.C. Gates, C.B.E. Gawith, P.G.R. Smith, 150 GHz of thermo-optic tuning in direct UV written silica-on-silicon planar Bragg grating, Electron. Lett. 45 (18) (2009) 954, https://doi.org/10.1049/el.2009.1305.

[17] Y. Bai, T. Vallée, T. Keller, Modeling of thermal responses for FRP composites under elevated and high temperatures, Compos. Sci. Technol. 68 (1) (2008) 47–56, https://doi.org/10.1016/j.compscitech.2007.05.039.

[18] G. B Vaggar, S. C Kamate, P. V Badyankal, Thermal properties characterization of glass fiber hybrid polymer composite materials, IJET 7 (34) (2018) 455, https://doi.org/10.14419/ijet.v7i3.34.19359.

[19] U. Berardi, N. Dembsey, Thermal and fire characteristics of FRP composites for architectural applications, Polymers (Basel) 7 (11) (2015) 2276–2289, https://doi.org/10.3390/polym7111513.

[20] Y. Yang, T. Vervust, S. Dunphy, S. Van Put, B. Vandecasteele, K. Dhaenens, L. Degrendele, L. Mader, L. De Vriese, T. Martens, M. Kaufmann, T. Sekitani, J. Vanfleteren, 3D multifunctional composites based on large-area stretchable circuit with thermoforming technology, Adv. Electron. Mater. 4 (8) (2018) 1800071, https://doi.org/10.1002/aelm.201800071.

[21] H.L. Rogers, S. Ambran, C. Holmes, P.G.R. Smith, J.C. Gates, In situ loss measurement of direct UV-written waveguides using integrated Bragg gratings, Opt. Lett. 35 (17) (2010) 2849–2851. OL.35.002849.

[22] F. R. M. Adikan, C. B. E. Gawith, P. G. R. Smith, I. J. G. Sparrow, G. D. Emmerson, and C. Riziotis, "Single-step fabrication of raised index X-couplers via direct UV writing," in *2006 Optical Fiber Communication Conference and the National Fiber Optic Engineers Conference*, 2006, p. 3 pp., doi: 10.1109/OFC.2006.215656.

[23] B.J. Smith, D. Kundys, N. Thomas-Peter, P.G.R. Smith, I.A. Walmsley, Phase-controlled integrated photonic quantum circuits, Opt. Express 17 (16) (2009) 13516–13525.

[24] F. Rafiq, et al., Direct UV written optical waveguides in flexible glass flat fiber chips, IEEE J. Sel. Top. Quantum Electron. 18 (5) (2012) 1534–1539.

[25] L. Thylén, A comparison of optically and electronically controlled optical switches, Appl. Phys. A Mater. Sci. Process. 113 (2) (2013) 249–256, https://doi.org/10.1007/s00339-013-7914-x.

[26] V. Sasikala, K. Chitra, All optical switching and associated technologies: a review, J. Opt. 47 (3) (2018) 307–317.